APL Materials

Solar blind Schottky photodiode based on an MOCVD-grown homoepitaxial β-Ga_2O_3 thin film

Cite as: APL Mater. **7**, 022527 (2019); https://doi.org/10.1063/1.5064471
Submitted: 04 October 2018 • Accepted: 16 January 2019 • Published Online: 07 February 2019

Fikadu Alema, Brian Hertog, Partha Mukhopadhyay, et al.

Solar blind Schottky photodiode based on an MOCVD-grown homoepitaxial β-Ga_2O_3 thin film

Cite as: APL Mater. 7, 022527 (2019); doi: 10.1063/1.5064471
Submitted: 4 October 2018 • Accepted: 16 January 2019 •
Published Online: 7 February 2019

Fikadu Alema,[1,a)] Brian Hertog,[1] Partha Mukhopadhyay,[2,3] Yuewei Zhang,[4] Akhil Mauze,[4] Andrei Osinsky,[1,a)] Winston V. Schoenfeld,[2,3] James S. Speck,[4] and Timothy Vogt[5]

AFFILIATIONS

[1]Agnitron Technology Incorporated, Eden Prairie, Minnesota 55346, USA
[2]CREOL, The College of Optics and Photonics, University of Central Florida, 4000 Central Florida Blvd., Orlando, Florida 32816, USA
[3]BRIDG, 200 NeoCity Way, NeoCity, Florida 34744, USA
[4]Materials Department, University of California, Santa Barbara, California 93106, USA
[5]Electrical and Computer Engineering, Saint Cloud State University, St. Cloud, Minnesota 56301, USA

[a)]**Authors to whom correspondence should be addressed:** Fikadu.Alema@agnitron.com and Andrei.Osinsky@agnitron.com

ABSTRACT

We report on a high performance Pt/$n^-Ga_2O_3$/$n^+Ga_2O_3$ solar blind Schottky photodiode that has been grown by metalorganic chemical vapor deposition. The active area of the photodiode was fabricated using ~30 Å thick semi-transparent Pt that has up to 90% transparency to UV radiation with wavelengths < 260 nm. The fabricated photodiode exhibited Schottky characteristics with a turn-on voltage of ~1 V and a rectification ratio of ~10^8 at ±2 V and showed deep UV solar blind detection at 0 V. The Schottky photodiode exhibited good device characteristics such as an ideality factor of 1.23 and a breakdown voltage of ~110 V. The spectral response showed a maximum absolute responsivity of 0.16 A/W at 222 nm at zero bias corresponding to an external quantum efficiency of ~87.5%. The cutoff wavelength and the out of band rejection ratio of the devices were ~260 nm and ~10^4, respectively, showing a true solar blind operation with an excellent selectivity. The time response is in the millisecond range and has no long-time decay component which is common in photoconductive wide bandgap devices.

Solar blind deep ultraviolet (DUV) photodetectors with a cutoff wavelength below ~280 nm have been widely studied for a variety of military and civilian applications, including flame sensing, missile interception, and air and water purification.[1–4] Wide bandgap materials such as MgZnO, AlGaN, and diamond have been investigated for their suitability for solar blind photodetector applications.[1,2,5–7] However, diamond has a restricted sensitivity range due to its wide bandgap (5.5 eV). Moreover, for MgZnO and AlGaN material systems, realizing true solar blindness is not straightforward due to challenges related to the growth of high quality materials with the required composition. In MgZnO, the structural dissimilarity between wurtzite ZnO and cubic MgO limits their solubility, promoting phase segregation.[8] In the past, the authors have applied a pulsed metalorganic chemical vapor deposition (MOCVD) method to grow single phase wurtzite MgZnO with a Mg content of 51% (E_g ~ 4.5 eV) on a ZnO buffer layer.[9] However, the presence of the ZnO buffer layer significantly reduced the out of band rejection ratio of the photodetector, making it difficult to achieve true solar blindness.[6] Similarly, the growth of Al rich AlGaN alloys requires a high substrate temperature that deteriorates the surface quality for Al content > 0.45.[10] From a practical point of view, it is desirable to find an alternative wide bandgap material that is easy to grow and demonstrates inherent absorption properties in the solar blind spectral region. One of the alternative material systems for DUV photodetection which has attracted a great deal of attention in recent years is β-Ga_2O_3.[11]

β-Ga_2O_3 is a wide bandgap oxide semiconductor widely investigated for applications in high power devices[12,13] and solar blind photodetectors.[14,15] The material has a large bandgap of ~4.9 eV and an estimated breakdown field of ~8 MV/cm.[16] A key advantage of β-Ga_2O_3 is the availability of free-standing β-Ga_2O_3 substrates fabricated using inexpensive melt techniques such as Floating Zone (FZ),[17] Edge-Defined Film-Fed Growth (EFG),[18,19] and Czochralski (CZ)[20,21] methods. Owing to these benefits, a large body of research on this material is focused on the study of power devices, including MESFETs,[16,22] Schottky diodes,[23,24] and MOSFETs.[22,25,26] Likewise, a significant body of work has been reported on Ga_2O_3 based photodetectors by growing epitaxial films on c-plane sapphire substrates by molecular beam epitaxy (MBE),[27,28] pulsed laser deposition (PLD),[29] and MOCVD[14] methods. However, these photodetectors are based on metal-semiconductor-metal (MSM) interdigitated electrode or back-to-back Schottky types which cannot operate without bias and suffer from slow response speed. To overcome these shortcomings, and fully exploit β-Ga_2O_3 for solar blind photodetection, one needs to develop vertical type photodetectors. However, only a few reports have directly demonstrated the fabrication of vertical photodiodes based on either bulk Ga_2O_3 substrate or epitaxial films.[15,30,31] Suzuki *et al.*[30] and Oshima *et al.*[31] have independently demonstrated vertical Schottky photodetectors based on bulk (100) β-Ga_2O_3 substrates showing high photoresponsivity under reverse bias voltage which was attributed to the presence of internal gain. On the other hand, we have recently reported a vertical Schottky photodiode based on plasma assisted MBE (PAMBE) grown Ge doped epitaxial β-Ga_2O_3 on a Sn doped (010) β-Ga_2O_3 substrate. The device showed a solar blind photodiode with a peak responsivity of 0.09 A/W at 230 nm with no applied bias and an out of band rejection ratio of 10^4.[15,32] Despite not being optimized, the performance of the device was comparable to that of commercially available photodetectors and true solar blindness was achieved. Similarly, Guo *et al.*[33,34] reported self-powered β-Ga_2O_3 based Schottky photodetectors by growing the films on non-native substrates such as ZnO and Nb doped $SrTiO_3$ using the RF magnetron sputtering method. In this work, we report on the first MOCVD grown lightly Si doped β-Ga_2O_3 based vertical Schottky photodiode. The device showed a true solar blind photodiode with a peak responsivity of 0.16 A/W and an out of band rejection ratio of 10^4, corresponding to an external quantum efficiency (EQE) of more than 85%.

High quality, homoepitaxial, lightly Si doped β-Ga_2O_3 was grown on a Sn doped (010) β-Ga_2O_3 substrate using an Agnitron Technology Agilis R&D MOCVD system. Triethylgallium (TEGa), 40 ppm of SiH_4 diluted in He, and O_2 (5 N) were used, respectively, as metalorganic precursors for Ga, Si, and oxidation. High purity Ar (6 N) was used as the carrier gas. First, a thin (~150 nm) heavily Si doped layer (~2×10^{18} cm^{-3}) was grown on the substrate followed by a 600 nm thick Ga_2O_3:Si layer [see Fig. 1(a)] at a growth rate of ~ 0.8 μm/h with a low targeted Si doping concentration of ~10^{16} cm^{-3}. The growth of the material in this study was conducted using optimized growth conditions that previously led to the realization of record room temperature electron mobility of 176 $cm^2/V\,s$[35] and low background doping concentrations (as low as 3×10^{15} cm^{-3}) in an unintentionally doped (UID) β-Ga_2O_3 epitaxial films.[36] Further details of the growth conditions can be found elsewhere.[37] The grown layer showed a smooth surface morphology with an RMS roughness of 0.54 nm, determined from the 2D AFM image in Fig. 2(a) over a 5×5 μm^2 scan area. The RMS value of the layer is comparable to the best values available in the literature for β-Ga_2O_3 layers grown by MBE[38,39] and MOVPE[40] despite using a growth rate over

FIG. 1. MOCVD grown β-Ga_2O_3 layer used for the study of vertical Schottky photodiode. (a) Schematic of the grown layer structure and cross-sectional view of the fabricated photodiode. The active layer is coated with 30 Å semi-transparent Pt metal. (b) Optical image showing the photomask used for the fabrication of the photodiode. The inner disk is the active area of the photodiode with a diameter of ~500 μm. (c) UV-visible transmission for Pt films deposited by the e-beam evaporation method on c-plane sapphire substrates with thickness ranging from 30 Å to 70 Å. These transmission data are not corrected for sapphire substrates which absorb ~20%-25% in the deep UV region.[45] For the 30 Å thick Pt window, the transmittance could reach up to 90% for radiation with wavelengths below 260 nm.

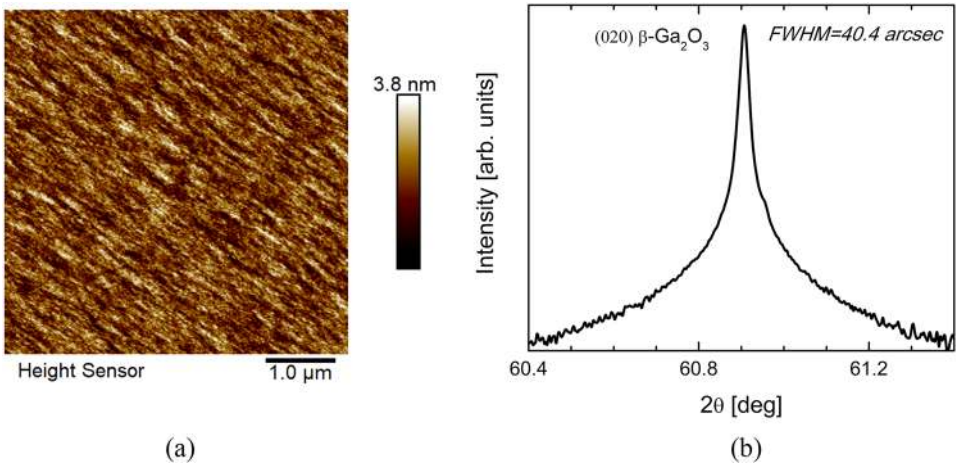

FIG. 2. (a) 2D AFM image showing the surface morphology and (b) HRXRD pattern in the ω–2θ mode of the (020) reflection of the β-Ga_2O_3:Si layer grown on the bulk n^+ β-Ga_2O_3 substrate for the photodiode.

three times higher. In Fig. 2(b), the high resolution x-ray diffraction (HRXRD) (020) peak of the epilayer is shown. The XRD full width at half maximum (FWHM) of the (020) peak is 40.4 arcsec which is comparable with bulk substrates.[41,42] The observed surface and structural quality show the capability of the MOCVD method to grow device quality Ga_2O_3 epitaxial layers with a significantly faster growth rate than other epitaxial techniques.[32,43,44]

The as-grown film was fabricated into vertical type Schottky photodiodes using standard lithography processes, as shown in Fig. 1(a). Ti(20 nm)/Al(100 nm)/Ni(50 nm) metal stack layers were evaporated on the back side of the Sn doped β-Ga_2O_3 (010) substrate followed by annealing at 500 °C for 60 s in N_2 to achieve a good Ohmic contact. Figure 1(b) shows the top view of an optical image of the photomask used to fabricate the vertical Schottky photodiodes. The Schottky contact was achieved with Pt(20 nm)/Ni(20 nm)/Au(130 nm) metal stack layers. The contact to the light absorbing (active) region of the device is semitransparent with an ~ 30 Å Pt electrode and has a diameter of 500 μm. The thickness of the Pt metal used in this work was selected by depositing Pt layers of various thicknesses on c-sapphire substrates using the e-beam deposition method. Figure 1(c) presents the transmission of the Pt layers without correcting for the sapphire substrate, showing an increase in the transmission of the Pt films with the decrease in thickness. For the 30 Å Pt coated active region used in this work, >65% transparency to the UV light at a wavelength below 260 nm is observed [Fig. 1(c)]. However, it is known that in the deep UV region, sapphire absorbs ~20%-25% of the light,[45] suggesting that actual transmission of this Pt window could be as high as 90% in the wavelength range of interest.

The doping concentration in the lightly doped Ga_2O_3:Si layer was estimated from capacitance-voltage measurement using a mercury CV probe (diameter of 735 μm) on a sample grown under the same conditions. Figures 3(a) and 3(b) show the C (capacitance per unit area) versus bias voltage and the charge distribution (N_d-N_a) depth profiles, respectively, for UID layers (samples A and B) and a lightly Si doped layer (sample C) at an excitation frequency of 100 kHz. All three samples (A, B, and C) were ~3.2 μm thick and grown on semi-insulating (Fe doped) (010) β-Ga_2O_3 substrates at the same growth rate as the Ga_2O_3:Si layer grown on a Sn doped (010) β-Ga_2O_3 substrate used for the fabrication of the photodiode. Additionally, sample C was doped to the same doping level as the Ga_2O_3:Si

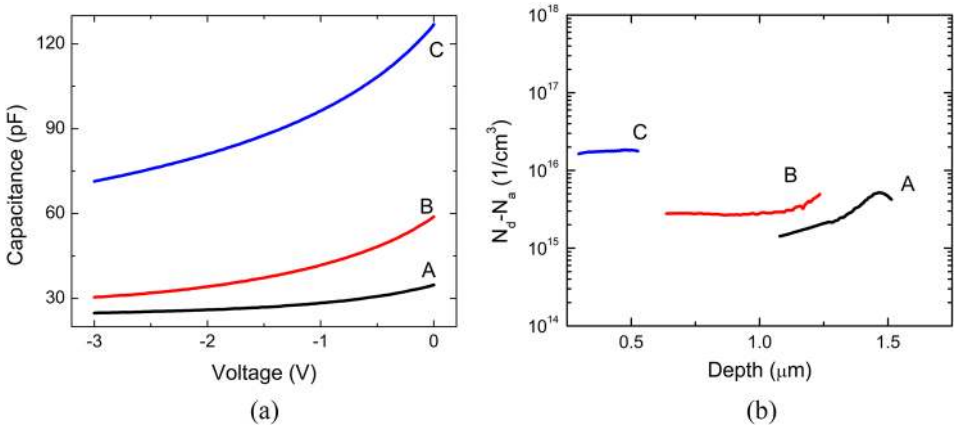

FIG. 3. CV characteristics measured by using a mercury probe at an excitation frequency of 100 kHz for samples A, B, and C grown on semi-insulating β-Ga_2O_3 substrates. Samples A and B are UID layers, while sample C is a lightly Si doped layer. (a) *C–V* plot and (b) extracted N_d-N_a versus depth profiles.

layer grown on the Sn doped (010) β-Ga_2O_3 substrate. The average N_d-N_a values for samples A, B, and C are 2.0×10^{15} cm^{-3}, 3.0×10^{15} cm^{-3}, and 1.8×10^{16} cm^{-3}, respectively, which are extracted assuming a dielectric constant of 10.[46] Room temperature Hall measurement conducted on sample C using Ti/Au Ohmic contact showed an electron mobility of ~120 cm^2/V s and a free carrier concentration of 2.6×10^{16} cm^{-3} which is comparable with the corresponding charge distribution obtained by CV measurement. Similar Hall measurement attempts for the UID layers were unsuccessful due to the resistivity of the layers. As seen in Fig. 3(b), the charge distribution shows a flat profile, except a slight variation for the UID layers, confirming a uniform charge distribution in the grown films.

To investigate the device performance in the DUV region, the response spectra of the photodiodes were measured using a 150 W Xenon lamp (Ushio UXL 150S) radiation source. The radiation passes through a scanning monochromator (Newport Cornerstone 130 1/8 m) and is focused onto the detector placed on a probe station. The photocurrent generated by using the detector was measured by using a lock-in amplifier (SR810 DSP) in sync with an optical chopper (Newport 75160 integrated chopper) at a frequency of 380 kHz. The measured spectra were then scaled by the responsivity profile and power spectrum obtained from an 818-UV Si photodetector. The current-voltage (I-V) characteristics under "dark" and "light" conditions were measured by using a Keysight B2987A electrometer/high resistance meter.

Figure 4(a) shows the dark current density-voltage (J-V) characteristics for the Schottky diode based on β-Ga_2O_3:Si grown on the bulk β-Ga_2O_3:Sn substrate. The curve shows excellent diode characteristics with a forward turn-on voltage of ~ 1.0 V and rectification ratio, (|J(+2 V)|/|J(−2 V)|), of ~10^8. For Schottky contacts, the current voltage characteristics are described by the thermionic emission equation given by[47]

$$J = J_0\left(\exp\left(\frac{qV}{nkT}\right) - 1\right), \quad (1)$$

$$J_0 = A^*T^2 \exp(-\varphi_B/kT), \quad (2)$$

where J_0 is the saturation current density, A^* is the effective Richardson constant, n is the ideality factor, q is the fundamental electric charge, k is the Boltzmann constant, T is the absolute temperature, and φ_B is the barrier height at the Pt/β-Ga_2O_3 junction. The A^* value in this analysis is estimated to be 41 A cm^{-2} K^{-2} using an electron effective mass of $0.342m_0$.[48] For a forward bias voltage, $V > 3kT/q$, Eq. (1) can be rearranged to extract the ideality factor n and barrier height φ_b using a linear fit to the ln J–V plot. Here, near unity n and φ_b values of 1.23 and 0.98 eV, respectively, were estimated for the Ga_2O_3:Si based vertical Schottky photodiode. These values are comparable with previously reported results for Pt/β-Ga_2O_3 junctions annealed at 200 °C.[23] Figure 4(b) shows the dark reverse J-V characteristics of the Schottky photodiode with a breakdown voltage, V_{br}, of 110 V. This is expected to be improved by using edge termination techniques and conducting the breakdown voltage measurement in a medium that prevents air breakdown such as Fluorinert solution. To identify the electrical breakdown mechanism and the potential use of the device as an avalanche photodiode similar to the GaN based photodiodes,[49] a thorough investigation including temperature dependent reverse bias IV measurements is needed and is beyond the scope of this work.

Figure 5(a) shows the current-time (I-t) measurements for a Schottky diode in the dark and under illumination at 250 nm without any external bias (zero bias). As shown in the figure, the device current increases sharply under UV light and remains constant (~72 pA) so long as the light remains on. Once the light is turned off, the current drops back to the dark value. The observation of photocurrent due to illumination clearly indicates that the device behaves as a Schottky barrier photodiode. The fast rise and fall in current with the state of illumination shows the fast response of the photodiode, while the absence of a long-time decay component is in contrast to what is commonly found in MSM photoconductive wide bandgap devices. The 10%–90% rise and fall times of the device were estimated to be ~0.5 s. Additionally, under dark conditions, the near zero bias leakage current is ~200 fA,

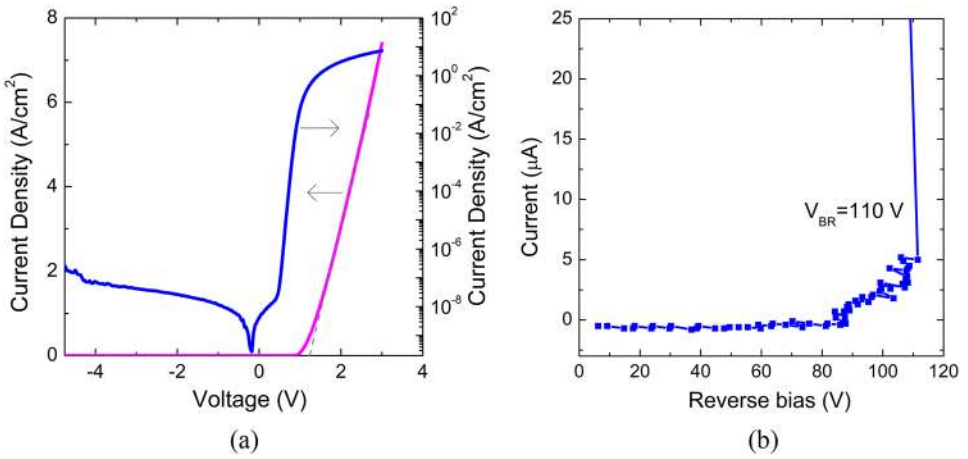

FIG. 4. (a) Current density-voltage (J-V) characteristics of the vertical Schottky diode based on β-Ga_2O_3:Si. (b) Reverse J-V characteristics showing a reverse breakdown voltage of 110 V. The ideality factor and potential barrier at the Pt/β-Ga_2O_3 junction were 1.23 and 0.98 eV, respectively.

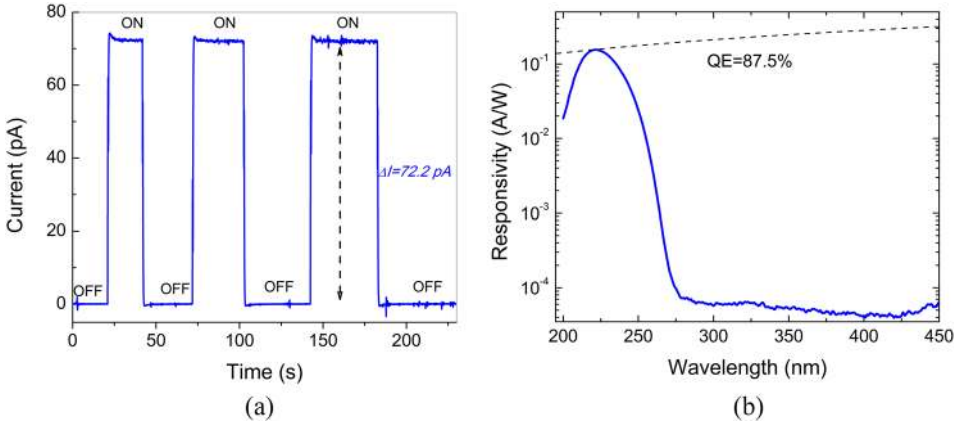

FIG. 5. (a) Zero bias current-time (I-t) characteristics of the vertical Schottky photodiode based on the β-Ga_2O_3:Si epitaxial film under dark and illuminated conditions. The photogenerated current under illumination is ~72 pA. (b) Zero bias spectral response of the Pt/$n^-Ga_2O_3/n^+Ga_2O_3$ vertical Schottky photodiode. The dashed line shows the wavelength dependent responsivity for a constant external quantum efficiency of 87.5%.

confirming, indirectly, that the device has a high signal to noise (S/N) ratio.

The room temperature absolute photoresponsivity of the vertical Schottky photodiode with no bias is shown in Fig. 5(b). The device showed a peak responsivity of ~0.16 A/W at 222 nm wavelength with a cutoff wavelength of 260 nm. The out of band rejection ratio (R222 nm/R350 nm) of the device is more than four orders of magnitude, showing the strong selectivity of the photodiode toward the solar blind spectral window. The external quantum efficiency (EQE) of the device was estimated using the relation, $EQE = 1240 \times R/\lambda$, where R and λ are the absolute responsivity and wavelength, respectively. Inserting the peak responsivity value and the corresponding wavelength into the equation, an EQE of 87.5% was calculated for the β-Ga_2O_3:Si based photodiode. The dashed line in Fig. 5(b) shows the wavelength dependent responsivity calculated using the constant EQE value estimated here.

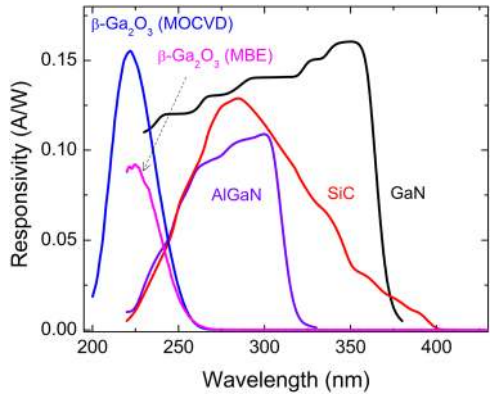

FIG. 6. Comparison of the photoresponsivity of the β-Ga_2O_3:Si photodiode grown using MOCVD (blue trace) with commercial devices based on GaN (black), SiC (red), AlGaN (purple), and an MBE grown β-Ga_2O_3:Ge photodiode (magenta) wide bandgap semiconductors. The data for GaN, AlGaN, and SiC are taken from Boston Electronics Corporation spec sheets for devices with part numbers AG38S-TO, AG32S, and SG01S, respectively. The MOCVD grown photodiode has shown a nearly doubled responsivity compared to similar structure grown by MBE.

Figure 6 compares the photoresponsivity for the MOCVD grown β-Ga_2O_3:Si photodiode with the β-Ga_2O_3:Ge photodiode reported by the authors[15] and commercial devices, including GaN, SiC, and AlGaN wide bandgap semiconductor materials (*Boston Electronics Corporation: the data for GaN, AlGaN, and SiC are for devices with part numbers AG38S-TO, AG32S, and SG01S, respectively*). As seen clearly from Fig. 6, the current device shows performance surpassing commercial devices. Moreover, it offers the added advantage of true solar blindness unlike available commercial devices. As compared to the MBE grown β-Ga_2O_3:Ge photodiode, the responsivity of the device grown using MOCVD has increased by ~1.8 times. This increase in photoresponsivity can be related to the quality of the MOCVD grown layer with a high electron mobility and reduced background impurity levels.[35,36]

In conclusion, high quality silicon doped β-Ga_2O_3 thin films were grown by the MOCVD technique and fabricated into vertical type Schottky photodiodes with a Pt/$n^-Ga_2O_3/n^+Ga_2O_3$ (010) structure. The photodiode showed excellent rectifying characteristics with a turn-on voltage of ~ 1 V, a rectification ratio of 10^8 at ±2 V, and a near zero bias leakage current of ~200 fA. The maximum responsivity was measured to be ~0.16 A/W at 222 nm, corresponding to a quantum efficiency of ~87.5%. The device exhibited an out of band rejection ratio of ~10^4 and had a cutoff wavelength of ~260 nm. The time response of the photodiode is in the millisecond range with no long-time decay component which is very common in the MSM photoconductive wide bandgap devices. The photodiode also showed a reverse breakdown voltage of 110 V.

The work at Agnitron Technology was supported by AFOSR and ONR programs through Grant Nos. FA9550-17-P-0029 and N00014-16-P-2058, respectively. Support at SCSU was provided through the state of MN DEED Program No. IVPP-17-0002. UCF would like to acknowledge support from the ARO under Project Award No. W911NF-17-S-0002. The work at UCSB was supported by AFOSR through Grant Nos. FA9550-18-1-0059 and FA9550-18-1-0479.

REFERENCES

[1]A. Osinsky, S. Gangopadhyay, B. W. Lim, M. Z. Anwar, M. A. Khan, D. V. Kuksenkov, and H. Temkin, Appl. Phys. Lett. **72**, 742 (1998).
[2]F. Alema, O. Ledyaev, R. Miller, V. Beletsky, B. Hertog, A. Osinsky, and W. V. Schoenfeld, Proc. SPIE **9749**, 97490Y (2016).
[3]E. Ozbay, N. Biyikli, I. Kimukin, T. Kartaloglu, T. Tut, and O. Aytür, IEEE J. Sel. Top. Quantum Electron. **10**, 742 (2004).
[4]A. Osinsky, S. Gangopadhyay, R. Gaska, B. Williams, M. A. Khan, D. Kuksenkov, and H. Temkin, Appl. Phys. Lett. **71**, 2334 (1997).
[5]A. Ohtomo, M. Kawasaki, T. Koida, K. Masubuchi, H. Koinuma, Y. Sakurai, Y. Yoshida, T. Yasuda, and Y. Segawa, Appl. Phys. Lett. **72**(19), 2466 (1998).
[6]F. Alema, B. Hertog, O. Ledyaev, D. Volovik, R. Miller, A. Osinsky, S. Bakhshi, and W. V. Schoenfeld, Sens. Actuators, A **249**, 263 (2016).
[7]A. BenMoussa, A. Soltani, K. Haenen, U. Kroth, V. Mortet, H. A. Barkad, D. Bolsee, C. Hermans, M. Richter, J. C. D. Jaeger, and J. F. Hochedez, Semicond. Sci. Technol. **23**(3), 035026 (2008).
[8]W. Yang, S. S. Hullavarad, B. Nagaraj, I. Takeuchi, R. P. Sharma, T. Venkatesan, R. D. Vispute, and H. Shen, Appl. Phys. Lett. **82**(20), 3424 (2003).
[9]F. Alema, O. Ledyaev, R. Miller, V. Beletsky, A. Osinsky, and W. V. Schoenfeld, J. Cryst. Growth **435**, 6 (2016).
[10]V. Kuryatkov, A. Chandolu, B. Borisov, G. Kipshidze, K. Zhu, S. Nikishin, H. Temkin, and M. Holtz, Appl. Phys. Lett. **82**(9), 1323 (2003).
[11]M. Orita, H. Ohta, M. Hirano, and H. Hosono, Appl. Phys. Lett. **77**, 4166 (2000).
[12]M. Higashiwaki, K. Sasaki, A. Kuramata, T. Masui, and S. Yamakoshi, Phys. Status Solidi A **211**(1), 21 (2014).
[13]K. Sasaki, A. Kuramata, T. Masui, E. G. Víllora, K. Shimamura, and S. Yamakoshi, Appl. Phys. Express **5**(3), 035502 (2012).
[14]F. Alema, B. Hertog, O. Ledyaev, D. Volovik, G. Thoma, R. Miller, A. Osinsky, P. Mukhopadhyay, S. Bakhshi, H. Ali, and W. V. Schoenfeld, Phys. Status Solidi A **214**, 1600688 (2017).
[15]F. Alema, B. Hertog, A. Osinsky, P. Mukhopadhyay, M. Toporkov, W. V. Schoenfeld, E. Ahmadi, and J. Speck, Proc. SPIE **10105**, 101051M (2017).
[16]M. Higashiwaki, K. Sasaki, A. Kuramata, T. Masui, and S. Yamakoshi, Appl. Phys. Lett. **100**(1), 013504 (2012).
[17]Y. Tomm, J. M. Ko, A. Yoshikawa, and T. Fukuda, Sol. Energy Mater. Sol. Cells **66**, 369 (2001).
[18]H. Aida, K. Nishiguchi, H. Takeda, N. Aota, K. Sunakawa, and Y. Yaguchi, Jpn. J. Appl. Phys., Part 1 **47**(11R), 8506 (2008).
[19]A. Kuramata, K. Koshi, S. Watanabe, Y. Yamaoka, T. Masui, and S. Yamakoshi, Jpn. J. Appl. Phys., Part 2 **55**(12), 1202A2 (2016).
[20]Z. Galazka, K. Irmscher, R. Uecker, R. Bertram, M. Pietsch, A. Kwasniewski, M. Naumann, T. Schulz, R. Schewski, D. Klimm, and M. Bickermann, J. Cryst. Growth **404**, 184 (2014).
[21]Z. Galazka, R. Uecker, D. Klimm, K. Irmscher, M. Naumann, M. Pietsch, A. Kwasniewski, R. Bertram, S. Ganschow, and M. Bickermann, ECS J. Solid State Sci. Technol. **6**(2), Q3007 (2017).
[22]N. Moser, J. McCandless, A. Crespo, K. Leedy, A. Green, A. Neal, S. Mou, E. Ahmadi, J. Speck, K. Chabak, N. Peixoto, and G. Jessen, IEEE Electron Device Lett. **38**(6), 775 (2017).
[23]M. Higashiwaki, K. Konishi, K. Sasaki, K. Goto, K. Nomura, Q. T. Thieu, R. Togashi, H. Murakami, Y. Kumagai, B. Monemar, A. Koukitu, A. Kuramata, and S. Yamakoshi, Appl. Phys. Lett. **108**(13), 133503 (2016).
[24]J. Yang, S. Ahn, F. Ren, S. J. Pearton, S. Jang, and A. Kuramata, IEEE Electron Device Lett. **38**, 906 (2017).
[25]A. J. Green, K. D. Chabak, E. R. Heller, R. C. Fitch, M. Baldini, A. Fiedler, K. Irmscher, G. Wagner, Z. Galazka, S. E. Tetlak, A. Crespo, K. Leedy, and G. H. Jessen, IEEE Electron Device Lett. **37**(7), 902 (2016).
[26]M. H. Wong, K. Sasaki, A. Kuramata, S. Yamakoshi, and M. Higashiwaki, IEEE Electron Device Lett. **37**(2), 212 (2016).
[27]O. Takayoshi, O. Takeya, and F. Shizuo, Jpn. J. Appl. Phys., Part 1 **46**(11R), 7217 (2007).
[28]A. S. Pratiyush, S. Krishnamoorthy, S. V. Solanke, Z. Xia, R. Muralidharan, S. Rajan, and D. N. Nath, Appl. Phys. Lett. **110**, 221107 (2017).
[29]Y. Fei-Peng, O. Sin-Liang, and W. Dong-Sing, Opt. Mater. Express **5**(5), 1240 (2015).
[30]R. Suzuki, S. Nakagomi, Y. Kokubun, N. Arai, and S. Ohira, Appl. Phys. Lett. **94**(22), 222102 (2009).
[31]T. Oshima, T. Okuno, N. Arai, N. Suzuki, S. Ohira, and S. Fujita, Appl. Phys. Express **1**, 011202 (2008).
[32]R. Miller, F. Alema, and A. Osinsky, in *Compound Semiconductor* (Compound Semiconductor, 2018), Vol. 24, p. 18.
[33]D. Y. Guo, H. Z. Shi, Y. P. Qian, M. Lv, P. G. Li, Y. L. Su, Q. Liu, K. Chen, S. L. Wang, C. Cui, C. R. Li, and W. H. Tang, Semicond. Sci. Technol. **32**, 03LT01 (2017).
[34]D. Guo, H. Liu, P. Li, Z. Wu, S. Wang, C. Cui, C. Li, and W. Tang, ACS Appl. Mater. Interfaces **9**(2), 1619 (2017).
[35]Y. Zhang, F. Alema, A. Mauze, O. S. Koksaldi, R. Miller, A. Osinsky, and J. Speck, APL Mater. **7**, 022506 (2019).
[36]A. Osinsky, Semiconductor Today **13**, 76 (2018).
[37]F. Alema, B. Hertog, A. Osinsky, P. Mukhopadhyay, M. Toporkov, and W. V. Schoenfeld, J. Cryst. Growth **475**, 77 (2017).
[38]K. Sasaki, M. Higashiwaki, A. Kuramata, T. Masui, and S. Yamakoshi, J. Cryst. Growth **392**, 30 (2014).
[39]K. Sasaki, M. Higashiwaki, A. Kuramata, T. Masui, and S. Yamakoshi, J. Cryst. Growth **378**, 591 (2013).
[40]M. Baldini, M. Albrecht, A. Fiedler, K. Irmscher, R. Schewski, and G. Wagner, ECS J. Solid State Sci. Technol. **6**(2), Q3040 (2016).
[41]D. Gogova, M. Schmidbauer, and A. Kwasniewski, CrystEngComm **17**(35), 6744 (2015).
[42]S. Rafique, M. R. Karim, J. M. Johnson, J. Hwang, and H. Zhao, Appl. Phys. Lett. **112**, 052104 (2018).
[43]R. Miller, F. Alema, and A. Osinsky, paper presented at the CS-MANTECH, Austin, Texas, 2018.
[44]R. Miller, F. Alema, and A. Osinsky, IEEE Trans. Semicond. Manuf. **31**(4), 467 (2018).
[45]E. R. Dobrovinskaya, L. A. Lytvynov, and V. Pishchik, *Sapphire* (Springer, New York, NY, USA, 2009), p. 85.
[46]M. Passlack, N. E. J. Hunt, E. F. Schubert, G. J. Zydzik, M. Hong, J. P. Mannaerts, R. L. Opila, and R. J. Fischer, Appl. Phys. Lett. **64**, 2715 (1994).
[47]S. M. Sze and K. K. Ng, *Physics of Semiconductor Devices*, 3 ed. (John Wiley & Sons, Inc., Hoboken, NJ, 2007).
[48]H. He, R. Orlando, M. A. Blanco, R. Pandey, E. Amzallag, I. Baraille, and M. Rérat, Phys. Rev. B **74**(19), 195123 (2006).
[49]A. Osinsky, M. S. Shur, R. Gaska, and Q. Chen, Electron. Lett. **34**(7), 691 (1998).